Rare Met. (2018) 37(8):690–698
https://doi.org/10.1007/s12598-018-1091-1

RARE METALS
www.editorialmanager.com/rmet

Isothermal oxidation behavior of scandium and yttrium co-doped B2-type iron–aluminum intermetallics at elevated temperature

Dong-Qing Li*, **Li-Xian Zhou, Kuan-Jun Zhu, Jian Gu, Shu-Hui Zheng**

Received: 26 January 2018 / Revised: 4 June 2018 / Accepted: 6 June 2018 / Published online: 20 June 2018

Abstract B2 FeAl intermetallic compounds modified with reactive elements (REs) including Sc and Y were fabricated by vacuum arc-melting, and the isothermal oxidation behavior of the RE-doped alloys at 1373 K was investigated. Both Sc and Y single-doping significantly decrease the alumina film growth rate of the alloys. The alumina film growth rate of Sc + Y co-doped alloy even further reduces compared to that of the Sc and Y single-doped alloys. The synergistic effect produced by Sc + Y co-doping on the growth behavior of alumina was discussed. It could be anticipated that the combined additions of Sc and Y which have matched chemical properties might decrease the alumina film growth rate more effectively and provide FeAl alloys with enhanced oxidation resistance.

Keywords Ferritic aluminides; Reactive elements; Co-doping; Isothermal oxidation; Segregation

1 Introduction

Ferritic aluminides have been widely studied and commercially utilized in extensive industrial fields as structural materials at temperatures up to 1073 K over the last few decades [1–4]. Among these intermetallics, B2 FeAl has received increasing attention mainly attributed to its low density with respect to steels or Ni-based alloys, relatively low cost and ability to form a dense and continuous alumina film at temperatures above 1173 K, and it has been recognized to be perfectly competent for oxidation-resistant coatings in industrial applications such as electric power generation and aero-engine manufacturing [5–10]. However, the film generated on FeAl alloy spalls readily during high-temperature cyclic oxidation, which is probably due to the accumulation of growth stress and thermal stress and the weak adhesion of the film to the alloy substrate [11, 12].

To solve this problem, different rare earths including Hf, Zr, Y, La and Ce were employed as potent modifiers. Long-term cyclic oxidation testing results showed that the additions of REs with moderate doping level (0.05 at%–0.10 at%) not only improved the adhesion of the alumina film to the alloy substrate but also decreased the growth rate of the film [13, 14]. Efforts have also been made to clarify this beneficial reactive element effect (REE) on the oxidation resistance of such alumina-forming alloys, and a list of proposed mechanisms related to the improvement in alumina film adhesion includes: (1) preventing the growth of film/alloy interfacial voids and intensifying the interface by weakening the "sulfur effect" [14–17], (2) releasing the strain energy and eliminating the rumpling of the film by promoting the strain tolerance of the film caused by the growth of columnar oxide grains [13, 18], (3) anchoring the scale by "oxide pegs" formed at the film/alloy interface [12, 19] and (4) strengthening the film/alloy interfacial adhesion by participating in bonding across the interface [20, 21]. For the decrease in alumina film growth rate, a dynamic segregation theory was proposed which has been partially confirmed by using high-resolution electron microscopy (HREM) and Auger electron microscopy (AEM) [22–25]. It suggests that a continuous flux of RE ions diffusing from the alloy substrate to the film–alloy interface and then segregating on alumina grain boundaries

D.-Q. Li*, L.-X. Zhou, K.-J. Zhu, J. Gu, S.-H. Zheng
Department of Transmission and Transformation Engineering Mechanics, China Electric Power Research Institute, Beijing 102401, China
e-mail: lidongqing1016@163.com

to modify the alumina growth mechanism is essential to implement the decreasing effect.

Apart from above merits, a growing number of studies also confirmed that RE single-doping only produced a limited improving effect on the oxidation resistance of alumina-formers [26, 27]. According to previous reports, over-doping of REs was easily achieved which resulted in severe internal oxidation of alumina-forming alloys due to their low solid solubility and higher oxygen affinity than Al. However, too low doping content had no obvious effect on improving the oxidation performance of the alloys. Recently, simultaneous doping of two REs has been considered to resolve this contradiction. It is reported by Pint et al. [26] that Hf and Y co-doping further decreased the alumina film growth rate of the FeCrAl alloys with lower total amount compared to Hf and Y single-doping. An interesting work by Lan et al. [28] revealed that more effective reduction in alumina film growth rate was obtained by combined additions of Dy and Pt in (Co, Ni)-based alloys. Moreover, combinations of Hf and Zr as well as Y and La are already doped in B2 NiAl alloys to realize enhanced oxidation resistance [29]. This RE co-doping strategy optimized the oxidation performance of alumina-forming alloys and allowed the total amount of RE additions to be minimized, thereby weakening internal oxidation. In spite of these persuasive findings, the essence of synergistic effect between two REs is not yet clarified and intensive research on the oxidation behavior of RE co-doped FeAl alloys is rarely conducted.

In the present work, Sc/Y-doped B2 FeAl alloys were produced by vacuum arc-melting. The isothermal oxidation test at 1373 K was performed, and a comparative research was carried out to investigate the roles of Sc and Y in affecting the growth behavior of alumina and to establish fundamental understanding of the synergistic effect between two REs on the oxidation performance of alumina-formers.

2 Experimental

Sc/Y-doped B2 FeAl alloys were used as testing alloys. The nominal doping level of each RE was ascertained according to the literature values [12, 17–20, 23–31]. Since RE atoms preferentially occupy Al lattice sites when squeezing into the FeAl lattice [32], the chemical compositions of testing alloys were designed as Fe–40Al (blank alloy), Fe–39.9Al–0.1Sc, Fe–39.9Al–0.1Y and Fe–39.9Al–0.05Sc–0.05Y (all in at%). Elemental metal bulks including Fe (purity 99.99 wt%), Al (purity 99.99 wt%), Sc (purity 99.9 wt%) and Y (purity 99.5 wt%) were employed as starting materials. A WK-2-type arc-melting furnace was utilized for alloy preparation. Low-density Al bulks were placed in the bottom of the melting crucible, and other high-density bulks were placed in the top. All the alloy ingots were melted five times with the melting current of 1200 A to guarantee sufficient alloying and subsequently annealed at 1473 K for 24 h in argon atmosphere. Chemical composition analysis of the as-annealed alloys was carried out by an inductively coupled plasma atomic emission spectrometer (ICP-AES, Plasma2000, China), and results are listed in Table 1. Specimens for isothermal oxidation testing were cut into 20 mm × 10 mm × 2 mm, ground to an 800-grit SiC finish and ultrasonically cleaned in alcohol and acetone, respectively.

Isothermal oxidation test was conducted in a thermal gravimetric analyzer (TGA, Thermax 700, Thermo Cahn) equipped with a gas flow system to allow reaction gas flowing into the chamber automatically, and the gas flow was kept at 30 ml·min^{-1}. Each specimen was hung in a pre-annealed alumina crucible by Pt wire to capture oxide spalls and immersed in dry, flowing O_2 at 1373 K for 50 h. Weight gain was automatically measured by an electronic balance with the precision of 1×10^{-5} g. The final mass gain for each alloy was determined based on an average value of three specimens' weight gains and corrected for the evaporation of Pt wire. To achieve morphology characterization of the oxides, specimens were put in a tube-type air furnace at 1373 K for desired oxidation time and taken out of the furnace after cooling to ambient temperature.

The microstructures of the alloys and the oxide films were characterized by a field emission scanning electron microscopy (FESEM, S4800, Hitachi) equipped with energy-dispersive spectroscopy (EDS). The chemical compositions of phases in the alloys and the films were determined by an electron probe micro-analyzer (EPMA, JXA-8100, JEOL). For the observation of cross-sectional morphologies, specimens after desired oxidation time were embedded in epoxy, ground to 3000-grit SiC finish and finely polished.

3 Results and discussion

3.1 Microstructure of as-annealed alloys

Before isothermal oxidation testing, the microstructure of the as-annealed Sc/Y-doped FeAl alloys was characterized

Table 1 Chemical compositions of as-annealed FeAl alloys determined by ICP-AES (at%)

Specimens	Fe	Al	Sc	Y
FeAl	Bal.	39.64	–	–
FeAl–Sc	Bal.	39.23	0.10	–
FeAl–Y	Bal.	39.72	–	0.09
FeAl–Sc–Y	Bal.	38.26	0.05	0.05

and the corresponding cross-sectional morphologies are shown in Fig. 1. Several bright precipitates are discovered along grain boundaries or within grain interiors in all the alloy substrates. EPMA detection reveals that these precipitates should be Sc/Y-rich phases (Table 2). Besides, all the precipitates exist in the co-doped alloy containing both Sc and Y rather than only one kind of them. This demonstrates that Sc and Y ions simultaneously precipitate into one phase during alloy preparation.

Owing to the solid solubility limit in FeAl lattice, excessive Sc and Y ions are inclined to precipitate accompanied with Fe or Al or both in the melting and casting process. As neighboring elements in the same family, Sc and Y have the same outermost electron configuration and stable valence state which allows them to substitute for each other when forming intermetallic compounds. In other words, Sc and Y ions combine with each other to form an integral ionic cluster and the precipitated intermetallics can be described as $Fe_pAl_q(Sc,Y)_r$. In terms of the above analysis, it can be inferred that Sc and Y ions first co-segregate on grain boundaries or within grain interiors according to their site preference and then co-precipitate into one phase during preparation of the co-doped alloy.

3.2 Growth kinetics of alumina films

Based on the classic works associated with the oxidation behavior of alumina-forming alloys [7, 10, 12, 17–20, 22–31, 33–35], the alumina film growth rate namely oxidation kinetics can be satisfactorily evaluated from the mass gain data which are recorded by weighting both of specimen and oxide spalls. Figure 2a shows the mass gain curves of the Sc/Y-doped FeAl alloys during 50-h isothermal oxidation at 1373 K. The Wagner theory suggests that the oxidation kinetics at high temperature is ordinarily controlled by the diffusion process of elements involved in oxidation reaction and generally follows a parabolic law:

Table 2 Chemical compositions of precipitates in as-annealed Sc/Y-doped FeAl alloys determined by EPMA in Fig. 1 (at%)

Regions	Fe	Al	Sc	Y
A	41.63	40.85	17.52	–
B	32.48	51.13	–	16.39
C	36.74	45.31	9.68	8.27
D	30.46	52.75	7.95	8.84

$$\Delta w^2 = k_p t \quad (1)$$

where Δw represents the mass gain per unit area, k_p represents the parabolic rate constant and t represents the oxidation time. According to Eq. (1), the curve of the square of mass gain versus oxidation time for each alloy was drawn, and the results are given in Fig. 2b. For the blank alloy, the highest mass gain and largest parabolic rate constant are obtained which were 1.72 $mg{\cdot}cm^{-2}$ and 2.44×10^{-5} $mg^2{\cdot}cm^{-4}{\cdot}s^{-1}$ after 50-h thermal exposure. Meanwhile, the Sc and Y single-doped alloys yield lower mass gains of 0.98 and 0.82 $mg{\cdot}cm^{-2}$ and smaller parabolic rate constants of 7.57×10^{-6} and 5.09×10^{-6} $mg^2{\cdot}cm^{-4}{\cdot}s^{-1}$, respectively. As compared to this, the mass gain further decreases (0.62 $mg{\cdot}cm^{-2}$) and the corresponding parabolic rate constant is 2.54×10^{-6} $mg^2{\cdot}cm^{-4}{\cdot}s^{-1}$ in the co-doped alloy. From the above results, it is clear that both Sc and Y single-doping significantly decrease the alumina film growth rate of FeAl alloys, and it is exciting that Sc + Y co-doping even further reduces the growth kinetics of the alumina film.

3.3 Growth mechanism of alumina films

Despite that the phenomenon of oxidation rate reduction caused by RE doping has been observed in a series of alumina-forming alloys such as FeAl, Fe_3Al and NiAl, the related mechanism is still in debate. Recently, a dynamic segregation theory was proposed by Pint et al. [23, 25]. They argued that the beneficial reactive element effect

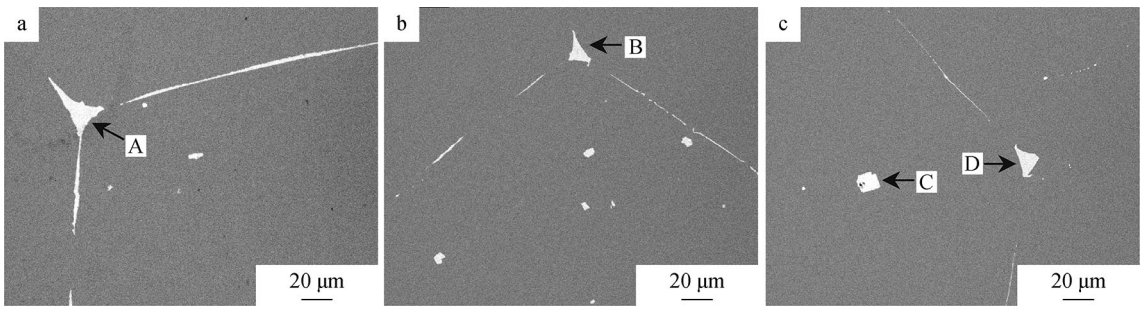

Fig. 1 FESEM-BSE images of polished cross-sections of as-annealed FeAl alloys: **a** FeAl–0.1 at%Sc, **b** FeAl–0.1 at%Y and **c** FeAl–0.05 at%Sc–0.05 at%Y

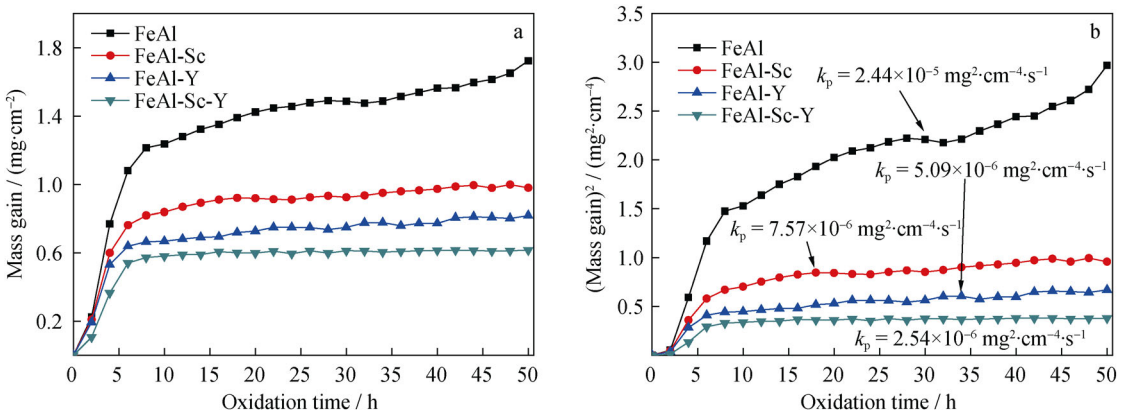

Fig. 2 **a** Mass gains (specimen + spall) and **b** their square for FeAl alloys during 50-h isothermal oxidation at 1373 K

(REE) on alumina film growth rate is essentially attributed to an outward transport behavior of RE ions under oxygen potential gradient during thermal exposure. It suggests that RE ions first migrate to the film–alloy interface rather than staying in the alloy substrate and then diffuse to the film–gas interface along alumina grain boundaries which are the predominant pathways for ion diffusion as grain boundary diffusion rate is much higher than crystal diffusion rate in alumina bulks at 1573 K or below [33]. Since Al ions diffuse along the same pathways to accomplish oxidation reaction, the slow diffusion of large RE ions seriously physically blocks the rapid diffusion of small Al ions and the inward diffusion of oxygen dominates the alumina growth mechanism instead. As anions normally display a lower diffusion rate than cations, decreased alumina film growth rate is achieved. Hence, the modification of alumina growth mechanism by a blocking effect should be mainly responsible for the decrease in alumina film growth rate.

The microstructure of the alumina film grown on each alloy was carefully examined, aiming to intuitively investigate the blocking effect produced by the outward migration of RE ions. Figure 3 shows the secondary electron (SE) plan-view images of the oxide films after 5-h isothermal oxidation at 1373 K. It is obvious that coarse ridge appears in the film on the blank alloy (Fig. 3a) which belongs to a typical structure of growing Al_2O_3 attributed to a growth mechanism dominated by the outward grain boundary diffusion of Al ions [36]. In contrast to this, fine close-compacted oxide grains are formed on all areas of the co-doped alloy surface (Fig. 3d), reflecting that Al outward diffusion is completely suppressed by co-doping Sc and Y. For the single-doped alloys, most of the alloy surfaces are also covered with granular oxides. However, the ridge structure is still found in the films, especially the Sc-doped alloy (Fig. 3b, c). This indicates that Sc and Y additions only inhibit the outward diffusion of partial Al ions and the cation transport still makes contribution to oxide film growth. Based on the above analysis, there is no doubt that the additions of Sc and Y do block the outward diffusion of Al ions which directly induce the modification of oxide morphology. Besides, it should be noted that no Sc/Y-rich oxides or Sc/Y-containing phases are observed on all the doped alloys. However, Sc and Y ions are still believed to first migrate to the alloy surface beneath the film in the initial oxidation period, but there might be no enough time for them to reach the outer surface of the film along oxide grain boundaries.

In this case, the back-scattered electron (BSE) cross-sectional images of the oxide films after prolonged oxidation time were investigated, and results are shown in Fig. 4. For the blank alloy, a rumpled film with the thickness of $\sim$ 10 μm is loosely bonded to the alloy substrate which results from the accumulation of growth stress during oxidation (Fig. 4a). Several white dispersions exist in the films on all the doped alloys except for FeAl–Y, on which some cluster-like phases occupy most areas of the films and one oxide peg is formed around them at the film–alloy interface which is considered as an enhancer for oxide film adhesion (Fig. 4b–d) [12, 19, 37]. EPMA detection implies that these particle-like and cluster-like phases should be Sc/Y-rich oxides (Table 3). These inspiring results manifest that a considerable quantity of Sc and Y ions diffuses from the film–alloy interface and segregate on oxide grain boundaries, significantly prohibiting the outward diffusion of Al ions. Since the inward diffusion of oxygen occurs simultaneously, an ion encounter takes place and Sc and Y ions are inevitably oxidized.

Figure 5 shows BSE plan-view image of the oxide film on the co-doped alloy after 50-h isothermal oxidation at 1373 K, representing the typical morphology of RE-doped Al_2O_3. Granular oxide grains with a similar size ($\sim$ 1 μm) are intimately distributed on the entire alloy surface. Furthermore, numerous white particles distinguish from aluminum oxide grains dispersed in the film (labeled by red arrow). EPMA results listed in Table 3 reveal that these

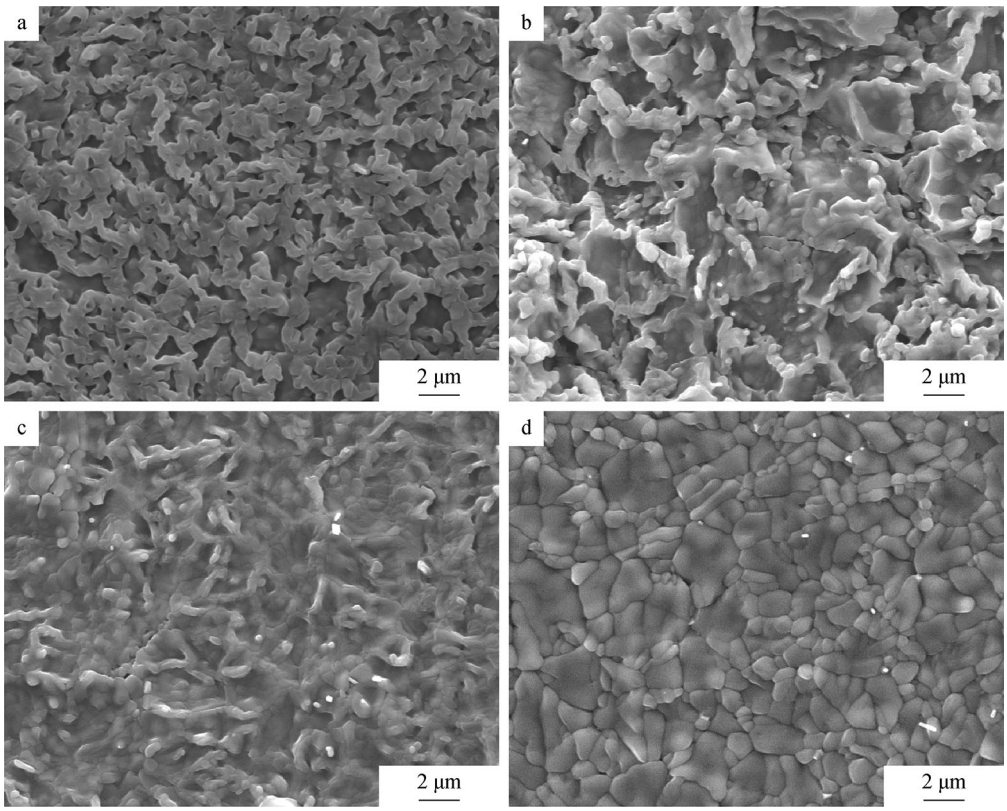

Fig. 3 FESEM-SE plan-view images of oxide films formed on FeAl alloys after 5-h isothermal oxidation at 1373 K: **a** blank FeAl, **b** FeAl–0.1 at%Sc, **c** FeAl–0.1 at%Y and **d** FeAl–0.05 at%Sc–0.05 at%Y

particles are enriched in both Sc and Y. Here, it should be noted that Sc and Y are simultaneously detected in regions C (Fig. 4d) and D (Fig. 5), which might be relevant to the co-segregation behavior of Sc and Y ions as mentioned in Sect. 3.1. Combined with the above observations, it is illustrated that Sc and Y ions act as an integral ionic cluster and simultaneously diffuse from the alloy and segregate on oxide grain boundaries and finally accumulate at the oxide film surface with oxidation time extending. And the nucleation of oxides enriched in both Sc and Y spontaneously occurs once their concentration level at the outer surface of the film reaches a critical value.

3.4 Synergistic effect between Sc and Y

In the above sections, a detailed oxidation kinetics comparison was conducted, showing that the Sc and Y single-doped FeAl alloys exhibit different characteristics in alumina film growth rate and the Sc + Y co-doped FeAl alloy acquires lower alumina film growth rate. Furthermore, a systematic oxide morphology characterization was performed, indicating that Sc and Y ions actually diffuse toward the oxide film surface from the alloy substrate, producing a blocking effect on the growth behavior of alumina as physical barriers. And the difference in blocking effect strength directly leads to distinct alumina film growth rate. Here, the total mass gain for each doped alloy after 50-h isothermal oxidation at 1373 K is represented with RE ion radius. On the basis of dynamic segregation theory, RE ions with larger radius must physically inhibit Al outward diffusion more effectively because larger ions occupy more areas of the diffusion pathways and diffuse at a lower rate. As expected, the results given in Fig. 6 reflect consistent tendency. In the present work, Y ions have larger radius, and the oxide film growth rate of the corresponding alloy is lower than that of the Sc-doped alloy. However, the Sc + Y co-doped alloy exhibits the lowest oxide film growth rate surprisingly, which is inconsistent with the prediction of the theory. This seeming contradiction suggests that a synergistic effect must exist between Sc and Y ions on the oxidation resistance of FeAl alloys which cannot be simply explained by the existing theory.

Actually, physical obstruction is only one aspect of the blocking effect, and chemical interaction inevitably exists between RE and Al ions. This interaction is considered to modify the electronic structure and enhance the diffusion activation energy of Al ions, thus further prohibiting Al outward diffusion. A concept of action radius can be adopted to more appropriately reflect the strength of

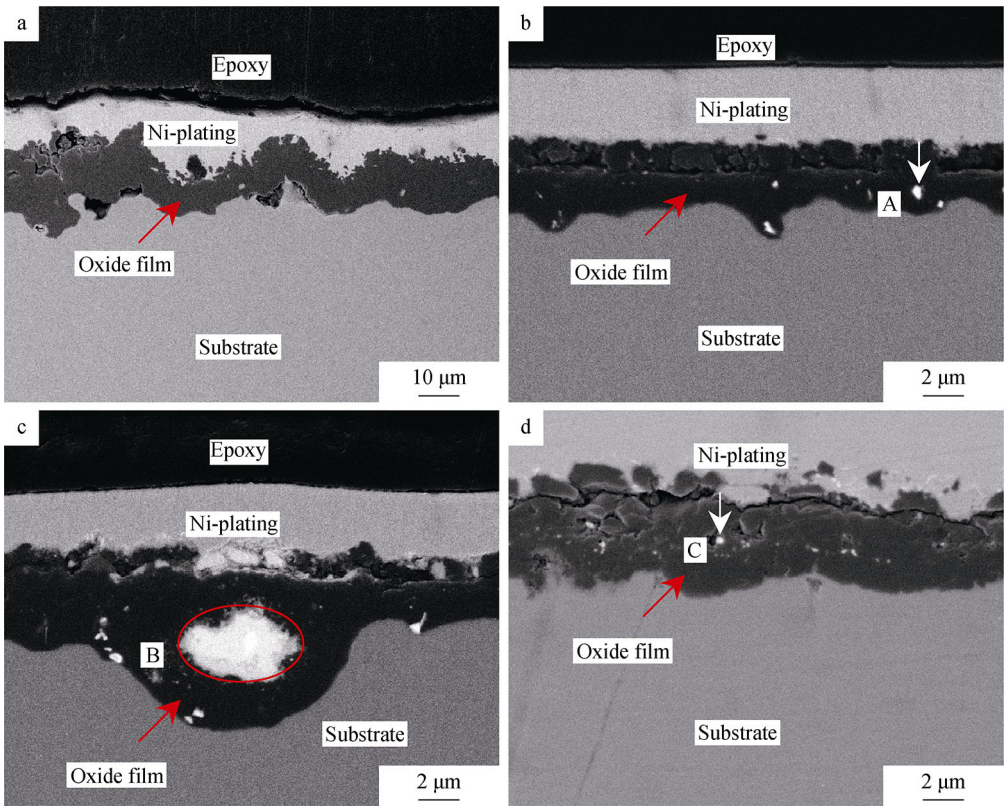

Fig. 4 FESEM-BSE images of polished cross-sections of oxide films formed on FeAl alloys after 50-h isothermal oxidation at 1373 K: **a** blank FeAl, **b** FeAl–0.1 at%Sc, **c** FeAl–0.1 at%Y and **d** FeAl–0.05 at%Sc–0.05 at%Y

Table 3 Chemical compositions of dispersed particles in oxide films after 50-h isothermal oxidation at 1373 K determined by EPMA (at%)

Regions	Fe	Al	O	Sc	Y
A in Fig. 4b	1.18	23.41	61.52	13.89	–
B in Fig. 4c	7.02	26.63	53.87	–	12.48
C in Fig. 4d	3.20	22.25	62.56	5.61	6.38
D in Fig. 5	–	23.31	65.53	5.27	5.89

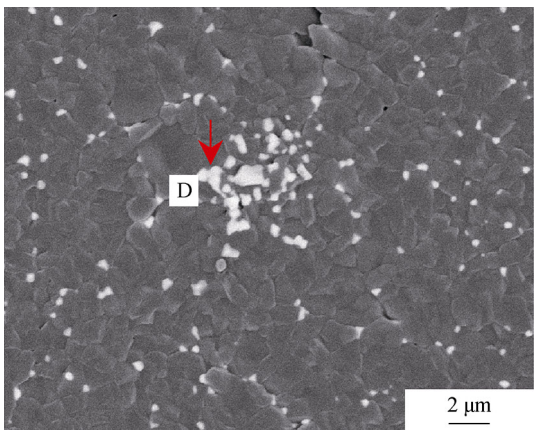

Fig. 5 FESEM-BSE plan-view image of oxide film formed on FeAl–0.05 at%Sc–0.05 at%Y alloy after 50-h isothermal oxidation at 1373 K

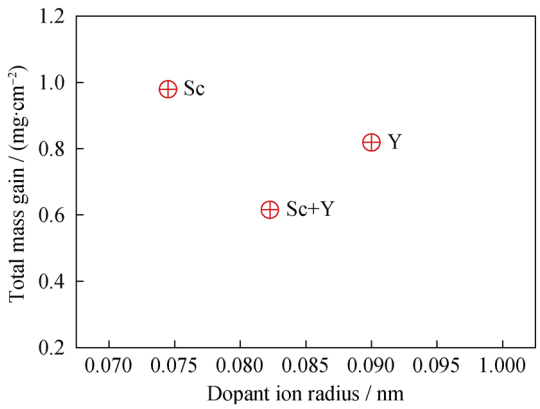

Fig. 6 Total mass gains (specimen + spalls) for Sc/Y-doped FeAl alloys plotted versus dopant ion radii after 50-h isothermal oxidation at 1373 K

blocking effect including physical obstruction and chemical interaction, and similar definition has also been proposed elsewhere [31]. As mentioned above, the Sc + Y ionic cluster diffuses outwardly along the cation diffusion pathways with oxidation time increasing and potently suppresses Al outward transport by physical obstruction and chemical interaction. Based on the present work, it is believed that the Sc + Y ionic cluster has stronger

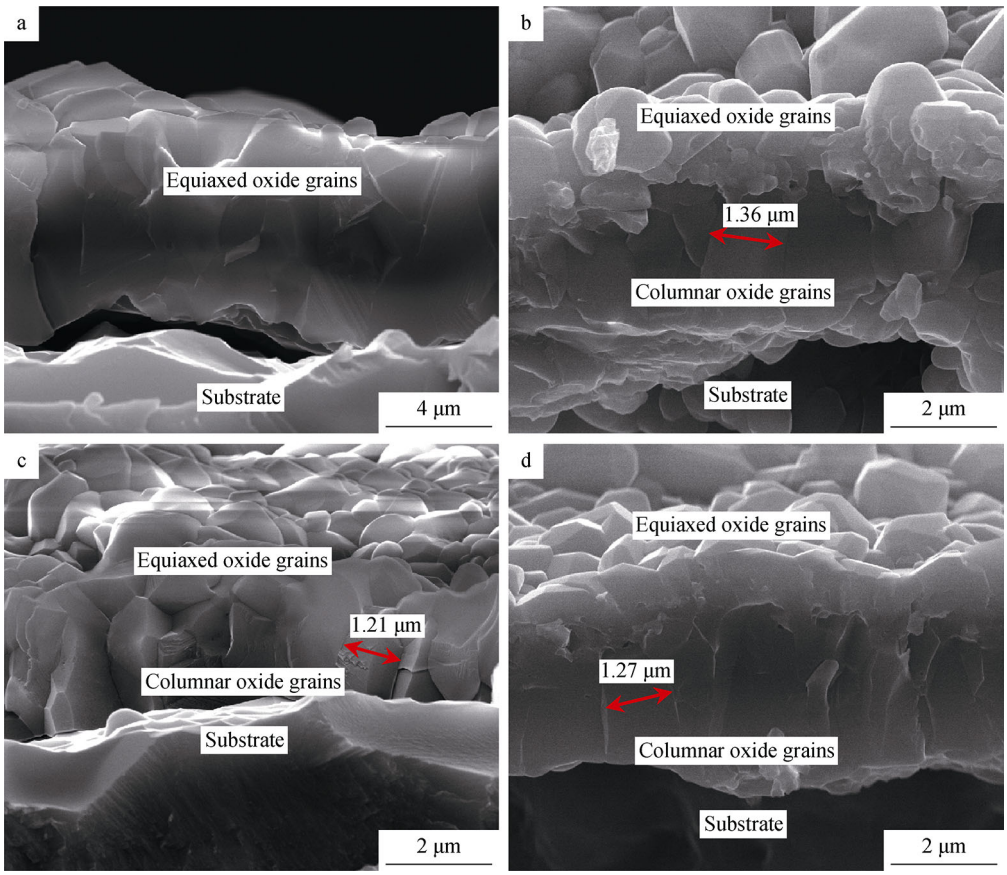

Fig. 7 FESEM-SE fracture images of oxide films formed on FeAl alloys after 50-h isothermal oxidation at 1373 K: **a** blank FeAl, **b** FeAl–0.1 at%Sc, **c** FeAl–0.1 at%Y and **d** FeAl–0.05 at%Sc–0.05 at%Y

chemical interaction with Al ion and larger action radius than two individual Sc or Y ions. Thus, the synergistic effect takes place between Sc and Y ions, which further reduces the alumina film growth rate.

Apart from the influence of RE ion radius on the strength of blocking effect, the quantity of RE ions segregating on the diffusion pathways of Al ions is also of importance. It is suggested that larger quantities of RE ions occupy more areas of the diffusion pathways, thus inhibiting Al outward diffusion more effectively. Figure 7 shows SE fracture images of the oxide films after 50-h isothermal oxidation at 1373 K. A thick film composed of equiaxed grains is observed on the blank alloy attributed to a simultaneous diffusion of Al and oxygen (Fig. 7a) [36]. In contrast to this, a double-layered film consisting of outer equiaxed grains and inner columnar grains is acquired on all the doped alloys due to a combination of inward growth mechanism and preferred growth direction induced by the grain boundary segregation of RE ions (Fig. 7b–d) [38]. In addition, the oxide films on all the doped alloys show similar grain size ($\sim$ 1.27 μm). Previous studies reported that grain refinement was achieved by RE ionic segregation on oxide grain boundaries due to a synergistic action of increase in heterogenous nucleation ratio and solute drag effect [23, 39, 40]. Therefore, the existence of columnar grains with similar size suggests that all the doped alloys exhibit a similar quantity of RE ionic segregation on oxide grain boundaries. Since different doped alloys display a similar RE ionic segregation level on the diffusion pathways of Al ions, the action ion radius becomes the first important factor influencing the strength of blocking effect.

Figure 8 shows a schematic illustration of how RE co-doping influences the growth behavior of alumina during isothermal oxidation, in which black arrows stand for the direction of cation diffusion from the alloy substrates to the oxide film surfaces, gray areas stand for alumina grain boundaries and spheres with different radii and colors stand for various cations during outward diffusion. For the single-doped FeAl alloys, Sc and Y ions occupy a considerable part of the diffusion pathways and show a lower diffusion rate, and consequently, the quantity and diffusion rate of Al ions both reduce. Experimental observations suggest that the blocking effect of RE ions on Al outward diffusion is composed of physical obstruction and chemical interaction, and this dual-effect phenomenon can be characterized by an action radius of a RE ion. In the illustration,

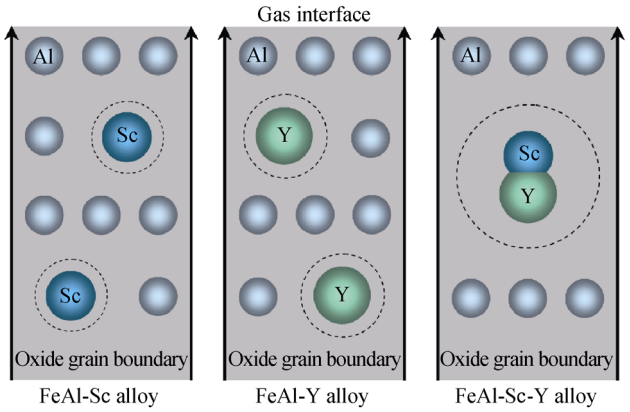

Fig. 8 A schematic illustration of how RE doping influences growth behavior of alumina on FeAl alloy during isothermal oxidation

this action radius is depicted as a dashed circle around each RE ion. It is obvious that the action radius is larger than actual radius for each RE ion due to its additional chemical interaction with Al ions. For the co-doped FeAl alloys, it is conceivable that Sc and Y ions interact with each other to form an integral ionic cluster, which has a larger action radius than two individual Sc or Y ions. Therefore, a synergistic effect arises between Sc and Y ions.

4 Conclusion

The microstructure and isothermal oxidation behavior of Sc/Y-doped B2 FeAl alloys at 1373 K were investigated. Cross-sectional morphologies show that Sc and Y are inclined to co-precipitate into one intermetallic phase during alloy melting and casting. Mass gain results indicate that Sc and Y single-doping effectively decrease the alumina film growth rate of the FeAl alloys by 43% and 52%. The Sc + Y co-doping even leads to the lowest growth rate of alumina film among the modified FeAl alloys (64% in decrease extent). It is proposed that Sc and Y ions perform as an integral ionic cluster which interacts with Al ions more intensely compared to two individual Sc or Y ions. Thus, a synergistic effect was produced, which further decreases the growth rate of alumina film on FeAl alloys.

Acknowledgements This research was financially supported by the Basic Research Program of State Grid (No. GCB17201500188).

References

[1] Ruan Y, Yan N, Zhu HZ, Zhou K, Wei B. Thermal performance determination of binary Fe–Al alloys at elevated temperatures. J Alloys Compd. 2017;701:676.
[2] Ohtsu N, Nomura A, Oku M, Shishido T, Wagatsuma K. X-ray photoelectron spectroscopic studies on oxidation behavior of nickel and iron aluminides under oxygen atmosphere at low pressures. Appl Surf Sci. 2008;254:5336.
[3] Zhang ZX, Li XY, Dong HS. Plasma-nitriding and characterization of $FeAl_{40}$ iron aluminide. Acta Mater. 2015;86:341.
[4] Airiskallio E, Nurmi E, Heinonen MH, Väyrynen IJ, Kokko K, Ropo M, Punkkinen MPJ, Pitkänen H, Alatalo M, Kollár J, Johansson B, Vitos L. High temperature oxidation of Fe–Al and Fe–Cr–Al alloys: the role of Cr as a chemically active element. Corros Sci. 2010;52:3394.
[5] Brito P, Pinto H, Kostka A. The crystallographic template effect assisting the formation of stable α-Al_2O_3 during low temperature oxidation of Fe–Al alloys. Corros Sci. 2016;105:100.
[6] Guilemany JM, Cinca N, Dosta S, Cano IG. FeAl and $NbAl_3$ intermetallic-HVOF coatings: structure and properties. J Therm Spray Technol. 2009;18:536.
[7] Lang FQ, Yu ZM, Gedevanishvili S, Deevi SC, Narita T. Cyclic oxidation behavior of Fe–40Al sheet. Intermetallics. 2004;12:451.
[8] Liu CT, George EP, Maziasz PJ, Schneibel JH. Recent advances in B2 iron aluminide alloys: deformation, fracture and alloy design. Mater Sci Eng A. 1998;258:84.
[9] Deevi SC, Sikka VK, Liu CT. Processing, properties, and applications of nickel and iron aluminides. Prog Mater Sci. 1997;42:177.
[10] DeVan JH, Tortorelli PF. The oxidation-sulfidation behavior of iron alloys containing 16–40 at% aluminum. Corros Sci. 1993;35:1065.
[11] Hou PY, Moskito J. Sulfur segregation to Al_2O_3–FeAl interfaces studied by field emission-Auger electron spectroscopy. Oxid Met. 2003;59(5):559.
[12] Xu CH, Gao W, Gong H. Oxidation behaviour of FeAl intermetallics. The effects of Y and/or Zr on isothermal oxidation kinetics. Intermetallics. 2000;8:769.
[13] Pint BA. Progress in understanding the reactive element effect since the Whittle and Stringer literature review. In: Proceedings of John Stringer Symposium on High Temperature Corrosion, ASM International; Novelty; 2003.9.
[14] Whittle DP, Stringer J. Improvements in high temperature oxidation resistance by additions of reactive elements or oxide dispersions. Philos Trans R Soc Lond Ser A. 1980;295:309.
[15] Wang L, Pan LL, Peng H, Guo HB, Gong SK. Cyclic oxidation behavior of Cr-/Si-modified NiAlHf coatings on single-crystal superalloy produced by EB-PVD. Rare Met. 2016;35(5):396.
[16] Yan K, Guo HB, Peng H, Gong SK. Oxidation behaviour of electron beam physical vapour deposition β-NiAlHf coatings at 1100 °C in dry and humid atmospheres. Rare Met. 2016;35(7):513.
[17] Xu CH, Gao W, Li S. Oxidation behaviour of FeAl intermetallics—the effect of Y on the scale spallation resistance. Corros Sci. 2001;43:671.
[18] Wang HF, Zhang YD, Shahzad S, Liu WB, Yang ZG, Zhang C. High temperature oxidation performance of CoNiCrAl alloy with different Sc contents. Chin J Rare Met. 2016;40(9):857.
[19] Xu CH, Gao W. Oxidation behaviour of FeAl intermetallics: effects of reactive elements on cyclic oxidation properties. Mater Sci Technol. 2001;17(3):324.
[20] Li DQ, Guo HB, Peng H, Gong SK, Xu HB. Improved alumina scale adhesion of electron beam physical vapor deposited Dy/Hf-doped β-NiAl coatings. Appl Surf Sci. 2013;283:513.
[21] Carling KM, Carter EA. Effects of segregating elements on the adhesive strength and structure of the α-Al_2O_3/β-NiAl interface. Acta Mater. 2007;55:2791.
[22] Heuer AH, Hovis DB, Smialek JL, Gleeson B. Alumina scale formation: a new perspective. J Am Ceram Soc. 2011;94(S):146.

[23] Pint BA. Experimental observations in support of the dynamic-segregation theory to explain the reactive-element effect. Oxid Met. 1996;45(1/2):1.
[24] Janda D, Fietzek H, Galetz M, Heilmaier M. The effect of micro-alloying with Zr and Nb on the oxidation behavior of Fe_3Al and FeAl alloys. Intermetallics. 2013;41:51.
[25] Pint BA, Alexander KB. Grain boundary segregation of cation dopants in α-Al_2O_3 scales. J Electrochem Soc. 1998;145(6):1819.
[26] Pint BA, More KL, Wright IG. The use of two reactive elements to optimize oxidation performance of alumina-forming alloys. Mater High Temp. 2003;20(3):375.
[27] Li DQ, Guo HB, Wang D, Zhang T, Gong SK, Xu HB. Cyclic oxidation of β-NiAl with various reactive element dopants at 1200°C. Corros Sci. 2013;66:125.
[28] Lan H, Zhang WG, Yang ZG. Investigation of Pt–Dy co-doping effects on isothermal oxidation behavior of (Co, Ni)-based alloy. J Rare Earths. 2012;30(9):928.
[29] Guo HB, Li DQ, Zheng L, Gong SK, Xu HB. Effect of co-doping of two reactive elements on alumina scale growth of β-NiAl at 1200°C. Corros Sci. 2014;88:197.
[30] Zhang YD, Zhang C, Wang HF, Yang ZG. Oxidation behaviour of CoNiCrAlY at 1000°C with Ce and Re additions. Chin J Rare Met. 2016;40(5):409.
[31] Pint BA, More KL, Tortorelli PF. Optimizing the imperfect oxidation performance of iron aluminides. Mater Sci Forum. 2001;369–372(1):411.
[32] Zheng YB, Wang F, Ai TT, Li C. Structural, elastic and electronic properties of B2-type modified by ternary additions FeAl-based intermetallics: first-principles study. J Alloys Compd. 2017;710:581.
[33] Pint BA. The oxidation behavior of Y_2O_3-dispersed β-NiAl. Oxid Met. 2004;61(3/4):273.
[34] Nowak K, Kupka M. High-temperature oxidation behaviour of B2 FeAl based alloy with Cr, Zr and B additions. Mater Chem Phys. 2012;132:902.
[35] Monceau D, Pieraggi B. Determination of parabolic rate constants from a local analysis of mass-gain curves. Oxid Met. 1998;50(5/6):477.
[36] Pint BA, Martin JR, Hobbs LW. ^{18}O/SIMS characterization of the growth mechanism of doped and undoped α-Al_2O_3. Oxid Met. 1993;39(3/4):167.
[37] Mennicke C, He MY, Clarke DR, Smith JS. The role of secondary oxide inclusions ("pegs") on the spallation resistance of oxide films. Acta Mater. 2000;48:2941.
[38] Guo HB, Zhang T, Wang SX, Gong SK. Effect of Dy on oxide scale adhesion of NiAl coatings at 1200°C. Corros Sci. 2011;53:2228.
[39] Cotell CM, Yurek GJ, Hussey RJ, Mitchell DF, Graham MJ. The influence of grain-boundary segregation of Y in Cr_2O_3 on the oxidation of Cr metal. Oxid Met. 1990;34(3/4):173.
[40] Cotell CM, Yurek GJ, Hussey RJ, Mitchell DF, Graham MJ. The influence of grain-boundary segregation of Y in Cr_2O_3 on the oxidation of Cr metal. II. Effects of temperature and dopant concentration. Oxid Met. 1990;34(3/4):201.